Available online at www.sciencedirect.com

ScienceDirect

Physics Procedia 83 (2016) 927 – 936

Physics Procedia

9th International Conference on Photonic Technologies - LANE 2016

Process influences on laser-beam melting of the magnesium alloy AZ91

Dominik Schmid[a,]*, Johanna Renza[a], Michael F. Zaeh[a], Johannes Glasschroeder[a]

[a]*Technical University of Munich, Insitute for Machine Tools and Industrial Management, Beim Glaspalast 5, 86153 Augsburg*

Abstract

Magnesium's great lightweight potential and high biocompatibility render laser-beam melting of this metal increasingly interesting. Despite recent research activities in this field, the properties thereby achieved are still inadequate for industrial or medical use. Low surface quality caused by powder sintered to parts' boundaries is one of the main problems. This effect is discussed theoretically and examined on single tracks of the magnesium alloy AZ91. Welding-penetration depth and width was measured on a magnesium plate with and without a powder layer. For the derivation of suitable process parameters, structures with incrementally increasing hatch distances were built and microscopically analyzed. The influence on defect percentage and hardness of the parts was determined based on specimens manufactured with different layer thicknesses. The influence of the oxygen content on solids was analyzed by varying the process atmosphere.

Peer-review under responsibility of the Bayerisches Laserzentrum GmbH

Keywords: laser beam melting; selective laser melting; magnesium; single tracks; sintering; layer thickness; residual oxygen content

1. Introduction

Magnesium is a silver-white metal with high oxygen affinity. Its low volumetric mass density of ρ_{Mg} = 1.74 g/cm³ renders it interesting for lightweight applications. Due to its high biocompatibility and resorbability, possible use in temporary medical implants is widely debated (Witte 2010). At the moment, magnesium is processed mainly by casting (Ehrenberger 2013). Processing with Laser Beam Melting (LBM) is currently being researched.

Initial investigations into the subject were published in 2010 (Ng et al; Savalani et al.) and 2011 (Ng et al.) by a research group at Hong Kong Polytechnic University. Single tracks of a preplaced, 800 µm thick magnesium powder

* Corresponding author. Tel.: +49-821-56883-55; fax: +49-821-56883-50 .
E-mail address: dominik.schmid@iwb.de

Peer-review under responsibility of the Bayerisches Laserzentrum GmbH
doi:10.1016/j.phpro.2016.08.097

layer were melted using a laboratory setup with a Nd:YAG laser (spot size 300 µm). Strong evaporations were observed during the process. Assumptions regarding the required line energy density were made based on the tracks' cohesion. Large areas of sintered powder were unavoidable with process parameters under which melting takes place. The basic microstructure, grain size, and hardness of melted single tracks were described. In 2012, Zhang et al. published investigations conducted with a commercial MCP Realizer 250 II SLM setup. A maximum part density of 82% proved obtainable using a magnesium-aluminum powder mixture containing 9% Al, a 50 µm layer thickness, and an 80 µm hatch distance while varying laser power, P_L, between 10 W and 110 W and laser scanning speed between 10 mm/s and 1000 mm/s. In 2013, the company Magnesium Elektron Powders published investigations into the laser metal deposition of magnesium and compared the resulting porosity using a coaxial powder feed to that from a preplaced powder bed (Tandon and Madan 2013). The Laser Zentrum Hannover research facility took an approach to minimizing evaporations using an overpressure atmosphere (Gieseke et al. 2013); however, the evaporations could not be minimized and the process became unstable (Gieseke et al. 2014). The ability to process pure Mg, MgCa0.8, and WE43 was compared (Gieseke et al. 2015). Wei et al. (2014) investigated the effects of variation in hatch distance and scanning velocity at a laser power (P_L) of 200 W on microstructure and mechanical properties. Manufacturing samples of magnesium alloy AZ91 with a density of 99.5% proved possible.

Nomenclature

A_N	Aspect ratio
b	Track width
E_L	Line energy density
E_V	Volume energy density
h_L	Hatch distance
l_z	Layer thickness
P_L	Laser power
R_z	Mean roughness depth
s	Weld penetration depth
v_L	Laser scanning speed
wt.%	Weight percentage
ρ	Volumetric mass density

2. Experimental procedures

The experiments were conducted using a ConceptLaser MLab R system with a built-in IPG ytterbium fiber laser (YLM-100). The maximum laser power, P_L, is 91 W (nominal 100 W); the spot size on the height of the building plate is approximately 50 µm. An argon process atmosphere with a residual O_2 content of about 0.3% was used unless stated otherwise. The starting material for the experiments was spherical, gas-atomized AZ91 (MgAl9Zn1) powder with the particle diameter ranging between 15 µm and 45 µm. The samples were built on a 1.5 mm thick AZ31 (MgAl3Zn1) metal sheet. To prevent movement and deformation, the metal sheet was fastened with countersunk screws to a thicker metal plate. The magnesium plate's absorption of the laser radiation was increased by roughening (Bergström et al. 2008) with sandpaper prior to the process ($R_z \approx 400$ µm). The samples were separated with a handsaw and embedded warm or cold depending on the type of sample. After grinding and polishing, the specimens were examined using confocal laser microscopy (Keyence VK9710) and scanning electron microscopy (Hitachi TM3030). Element concentrations were measured by energy dispersive spectroscopy (Bruker Quantax 70). Segmentation of the optical microscopy images based on the gray-level threshold (Pun 1980) was performed using the software ImageJ. Since other constituents besides pores, such as oxide films (Vander Voort 2004), can appear as dark regions on polished cross sections, the measured value is designated as a defect percentage rather than as a porosity. The laser scanning microscope was also used to optically measure the roughness of samples. For determining hardness, a universal testing machine (Zwick Roell Z 2.5) with a conical indenter

according to Vickers was used with a test load of 9.80 N and a holding time of 12 s. Ten indentations were made on each sample. Hardness was calculated by averaging the measured values.

To study the influence of laser powder and laser scanning speed on track formation and to contrast the influence of the powder on the process, single tracks without powder were initially exposed on the magnesium sheet. Increasing the complexity, single tracks with powder were exposed and analyzed. The influence of hatch distance at different laser scanning speeds was determined by generating structures with incremental hatch distances. After choosing a process-parameter combination that led to dense parts, the effect of layer thickness and oxygen content was measured.

Two common formulas are applied when comparing different parameter sets. Line energy density, E_L, is used to compare the energy input of single tracks, where P_L is the laser's output power and v_L the scanning speed with which the laser spot is moved.

$$E_L = \frac{P_L}{v_L} \tag{1}$$

Volume energy density, E_V, is used to compare the energy input for the remelting of more dimensional parts, with h_L being the hatch distance and l_z the layer height.

$$E_V = \frac{P_L}{v_L h_L l_z} \tag{2}$$

3. Examinations on single tracks and single layers

3.1. Melting of single tracks on a sheet plate

During laser beam melting, parts are generated by melting powder through the laser beam's line-wise movement. The metallurgical bonding within a single layer is created by an overlap of the width of melted tracks; the connection between different layers results from the weld depth exceeding the layer height. This relationship makes the weld track with its main parameters depth and width the basic element of laser-beam melted parts.

Since the powder affects multiple aspects of the process, welds produced under process conditions without powder were analyzed as a first step. Although the magnesium plate's absorption was increased by the already described roughening, it has to be kept in mind that the absorption of flat surfaces is lower compared to that of surfaces with a preplaced powder layer (Boley et al. 2015). The resulting melt tracks were analyzed regarding their homogeneity and their melt-pool depth and width through surface topology and cross-sections perpendicular to the scanning direction. The Laser power was varied between 15 W and 90 W in six steps to cover a broad process range. The Laser scanning speed was examined in 11 steps between 20 mm/s and 1000 mm/s resulting in line energy densities between 0.015 J/mm and 4.5 J/mm.

At a laser power of 15 W, forming (continuous) tracks independently of laser scanning speed proved impossible. For a laser power of 30 W, tracks exposed with velocities above 200 mm/s were partly interrupted. For high line energy density values (P_L = 75 W and 90 W, v_L = 20 mm/s), the melt track becomes irregularly shaped. For other parameter sets, a relatively even melt track was achievable (Fig. 1). Fig 2 shows weld-track variations. As expected, an examination of cross-sections shows that for all samples, welding-penetration depth and track width increase with laser power and decrease with laser scanning speed (Fig. 2). The aspect ratio, A_N, of track depth, s, to track width, b, shows the same alignment, since the welding-penetration depth is more dependent on the process parameters than the track width is. Different thresholds are in use to determine welding mode. In this work, welds with aspect values greater than 1 (Hügel et al. 2007, p. 222) are considered as keyhole mode and aspect values between 0.5 (King et al. 2014) and 1 as transition range. For aspect values lower than 0.5 thermal conduction mode melting is assumed.

Evaluation of the data shows that all tracks at 30 W and 45 W as well as tracks at 60 W with higher scanning speeds than 600 mm/s exhibit aspect values smaller than 0.5, which means that they were melted in thermal conduction mode. Tracks formed at 75 W and 90 W were built either in keyhole mode or in the transition range.

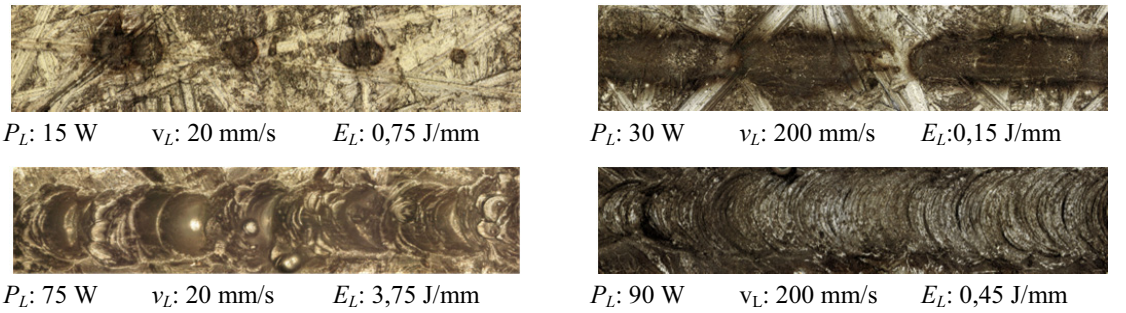

Fig. 1. Melt track morphologies.

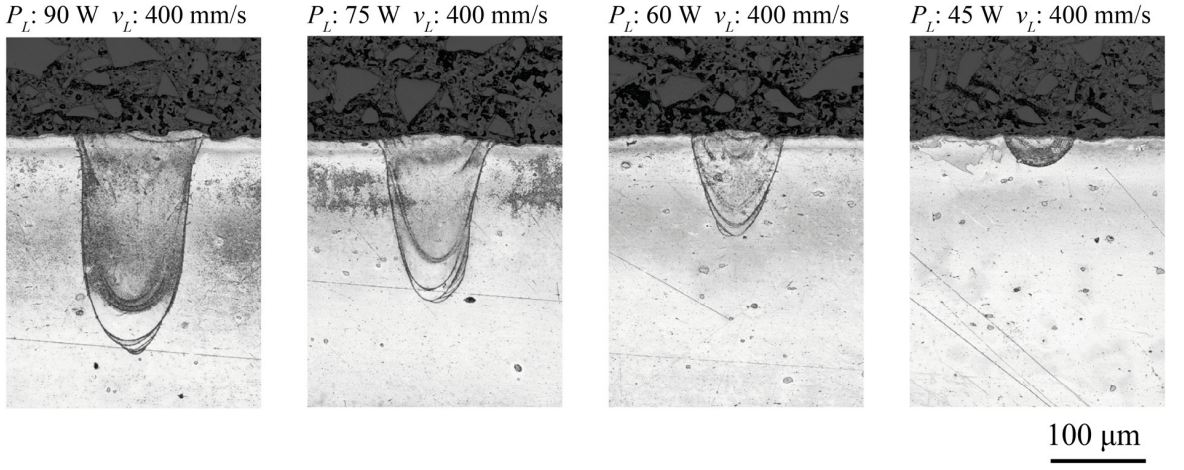

Fig. 2. Evolution of weld tracks at v_L = 400 mm/s and different laser powers P_L.

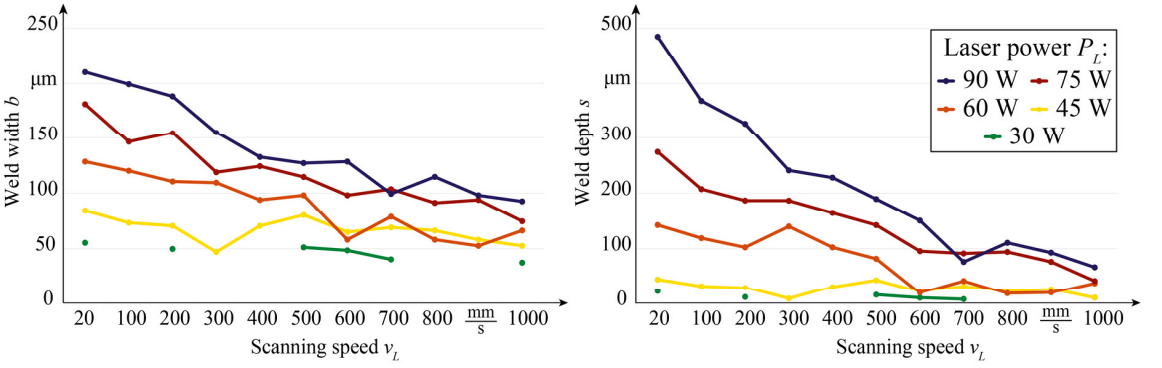

Fig. 3. Width and depth of single magnesium tracks on an AZ31 plate.

3.2. Melting of single tracks on powder layer

Increasing the complexity of the setup and the comparability to the additive process, the experiment was repeated melting ten layers of AZ91 powder to the AZ31 base plate. Despite some effort, a certain inhomogeneity in thickness of the powder layer could not be avoided, which limited the comparability of the track's height.

As stated in prior publications by Ng et al. and others, an extended zone of sintered particles can be observed on both sides of the melted track even at small line energies. Fig. 3 shows the top view of a single laser track taken with a scanning electron microscope. As in the test setup without powder the welding penetration depth and the track width increase with line energy density. With the same parameter set, the track width and depth are greater than in the setup lacking powder due to the higher absorption. Since absorption in keyhole melting is higher than that in conduction melting, the parameter combinations associated with conduction-mode melting are especially affected by the increased absorption through the powder layer (Fig. 4).

Within the examined range, no parameter set could be distinguished under which a track melts without particles being sintered. Extension of the sintered regions generally is greater for low scanning speeds. Compared to the melted track, the proportion of the sintered tracks increases with lower laser powers and scanning speeds. Fig. 5 shows the variation of the melt track and the sintered particles at a laser power P_L = 75 W and different laser scanning speeds v_L between 20 mm/s and 900 mm/s.

Particles sintering is also being oberserved at the generation of solids (Gieseke et al. 2015) where it affects surface quality and dimensional accuracy. It is therefore of special interest to understand the inducing mechanisms. The sintering of powder in several layers (as can be seen in Fig. 5 and Fig. 6) makes heat transfer by conduction unlikely because of the low conductivity of the loose, sintered powder. Sintering because of melt splashes is also improbable for the complex undercuts at the sintered material. One possible explanation for this is that the effect is related to the evaporations escaping the process zone. As the evaporations pass the particles of the powder bed, heat transfer takes place sintering the powder. Element distributions that can be found under some parameter combinations support this theory. Figure 7 shows one clear example. The element distribution of the unaffected AZ31 base plate [1] lies within the expected range. The observed aluminum content is notably greater in remelted material [2] than it is in the base plate (3%) or in the powder material (9%). This is caused by disproportionate magnesium evaporation. Even a greater aluminum content can be observed on the inner side of the sintered track [3]. Since it has the highest evaporation temperature of all alloying elements, it is the first to condense on the surrounding powder. The evaporated magnesium condenses in the following zone [4-6], leading to a lower aluminum content than that in the raw powder. At the track's outer limits [7, 8], the composition approaches the initial value. The observations could not been made as unambiguously on all samples, but the reason for the sintered tracks seems to apply generally, because the evaporations in the process can be observed under most parameter sets and the sintered-track patterns are comparable.

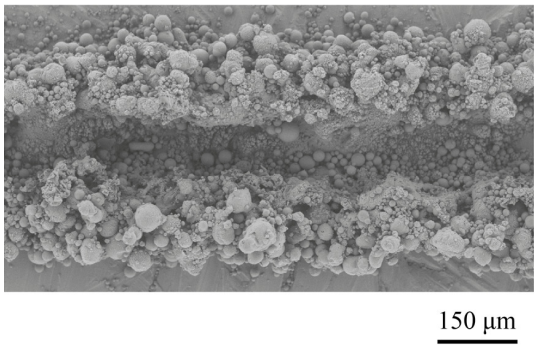

Fig. 4. SEM image of a single track (P_L: 30 W, v_L: 100 mm/s).

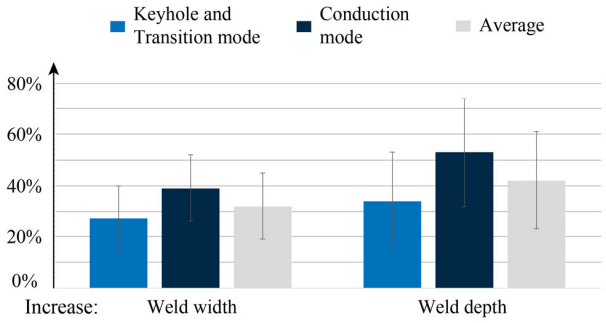

Fig. 5. Increase of the track geometry referred to tracks without powder.

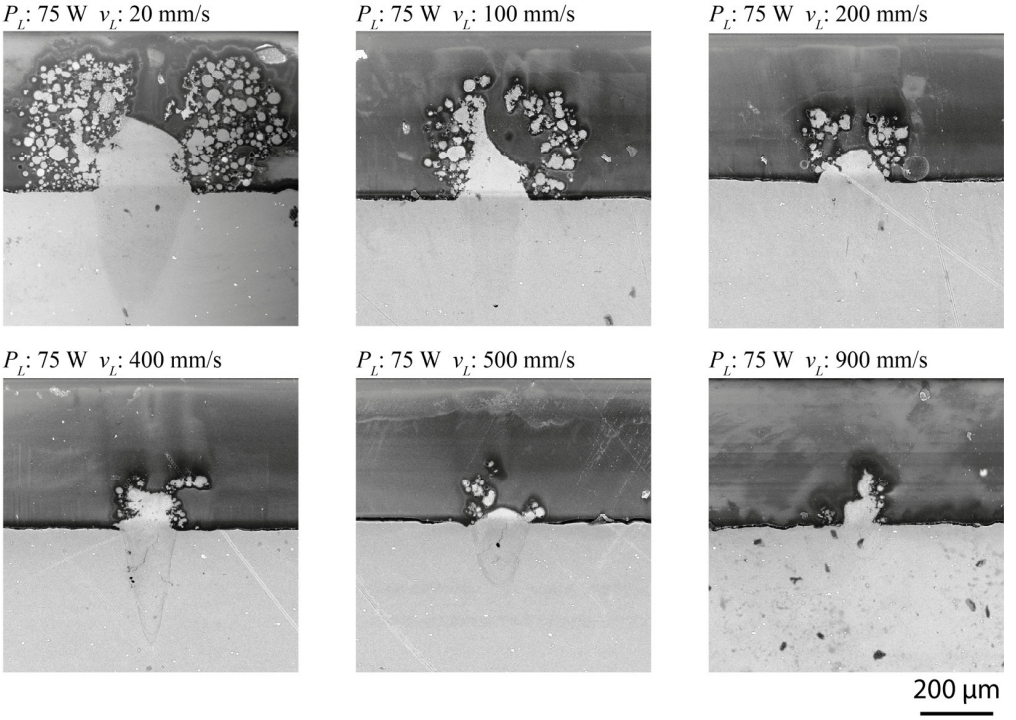

Fig. 6. Cross-sections of AZ91 tracks, at P_L = 75 W and different scanning speeds.

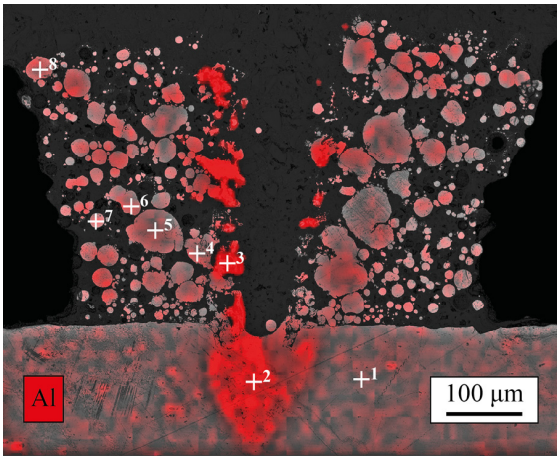

[wt. %]	Mg	Al	Zn
$+^1$	96.2	2.6	1.2
$+^2$	85.8	13.9	0.3
$+^3$	61.1	37.7	1.2
$+^4$	93.9	5.4	0.7
$+^5$	96.2	3.2	0.6
$+^6$	93.8	4.7	1.5
$+^7$	91.5	7.7	0.8
$+^8$	90.1	8.6	1.3

Fig. 7. Element mapping of aluminum and element composition by energy dispersive spectroscopy at different spots.

3.3. Melting of multiple track structures

In order to determine the influence of the hatch distance, laser tracks with incrementally decreasing distance were built at P_L = 90 W and different scanning speeds. Starting with 150 µm, the hatch distance was decreased to 10 µm

at a rate of 10 µm/mm, which resulted in a 14 mm long part. Unlike with conventional parts, the tracks were not exposed meander-like but were equally aligned to have approximately the same time interval along the whole track.

Single tracks can be clearly distinguished at the initial 150 µm hatch separation. Parts of the tracks are detectable within the structure independently of the scanning speed down to an 85 µm hatch separation. Therefore it could be concluded that this limit is not dependent on energy input but rather on the laser beam's (geometrical) energy distribution. For lower hatch spaces follows a zone of irregular sintering and a relatively smooth region with low deposition/high evaporation. Both areas can be quite small, and formulating a comprehensive rule to describe the transitions proved impossible. Fig. 8 shows the structure's evolution as a function of hatch separation at laser scanning speeds of 300 mm/s and 700 mm/s. The four zones describing the sample's surface structure as a function of energy input classified by Wei et al. could not be observed. A desired direct derivation of suitable process parameters for generating dense parts was not yet possible, but further investigations aiming at that will be undertaken.

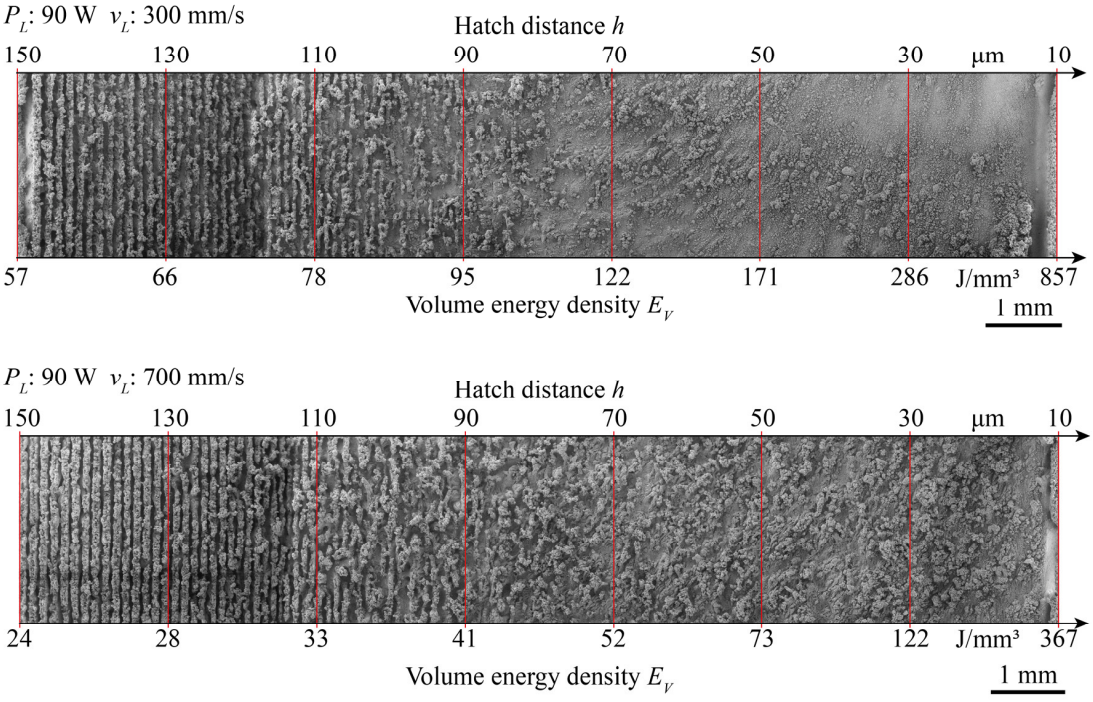

Fig. 8. Structures with varying hatch distance.

4. Examinations on solids

A parameter set with low defect percentage (P_L = 90 W, v_L = 700 mm/s, h_L = 35 µm, l_z = 30 µm) was selected as starting point for further investigations into building cubes using varying scanning speeds and laser powers. The resulting volume energy, E_v, of 122 J/mm³ is in accordance to Wei et al. (2014) where detailed investigations into the influence of energy input on solids are published.

4.1. Influences of the layer thickness

Layer thickness gains in importance when shifting from single-layer parts to multiple-layer parts. In contrast to other volume-energy-density parameters (Eq. 2), no investigations into this parameter have yet been published to the authors' knowledge. To determine the influence of the layer thickness, cubes were built with slices varying between 15 µm and 60 µm. The parts were randomly placed on one build plate so that whereas recoating took place for all samples, exposure was done selectively. This way the influence of energy input can be investigated minimizing secondary influences.

All layer thicknesses lead to rugged parts, but a visual inspection (Fig. 9) reveals that a layer thickness between 25 and 45 µm leads to the smoothest surfaces (R_z = 442 – 688 µm). Optical measurement results (in part indicated in the figure) show that the effect is quite pronounced for the XY surface, but cube surfaces facing toward the coating direction are also influenced.

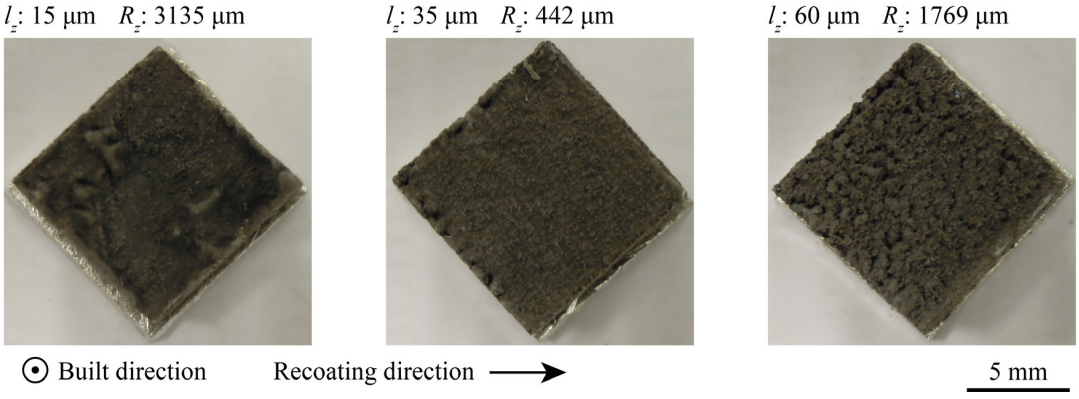

Fig. 9. Surface quality at different layer thicknesses.

For the parameter set used, a variation of the layer thickness between 15 µm and 45 µm does not seem to have significant influence on the defect percentage value or hardness. A layer thickness of 50 µm seems to be a clear limit where the defect-percentage value increases sharply and hardness declines. The measured values are depicted in Fig. 10a. The resulting range complies with the range where other materials are processed. Comparing the value to the weld depth of the single tracks (with powder layer: s = 140 µm) it is probable that the limitation in layer height is less related to the amount of energy input and more to the powder fraction and energy distribution. Since the energy density, E_V, could be varied in a relatively broad range between 82 J/mm³ and 245 J/mm³ without affecting part quality, the process seems less sensitive to a variation of the energy input via layer height than to the variation of other process parameters.

4.2. Influences of the oxygen-content

Because of the magnesium's high oxygen affinity, the influence of the process atmosphere on the sample is subject to controversial discussion. To determine the influence, samples were built under the standard parameter set in a process atmosphere having between 0.09% and 0.60% residual oxygen content. The defect percentage was evaluated and the sample's hardness tested after grinding and polishing. The measured values (Fig. 10b) show small variations that are within the experimental setup's limits of accuracy. It can therefore be concluded that there is no influence on sample hardness and density within the examined range. The impact on microstructure, amount of oxygen enclosed within the solid, and mechanical properties should be covered in future investigations. The influence of a significantly lower oxygen content may also represent a promising field of study, but a different

experimental setup will be needed since the 0.09% of residual oxygen content achieved is a restriction of the LBM system used.

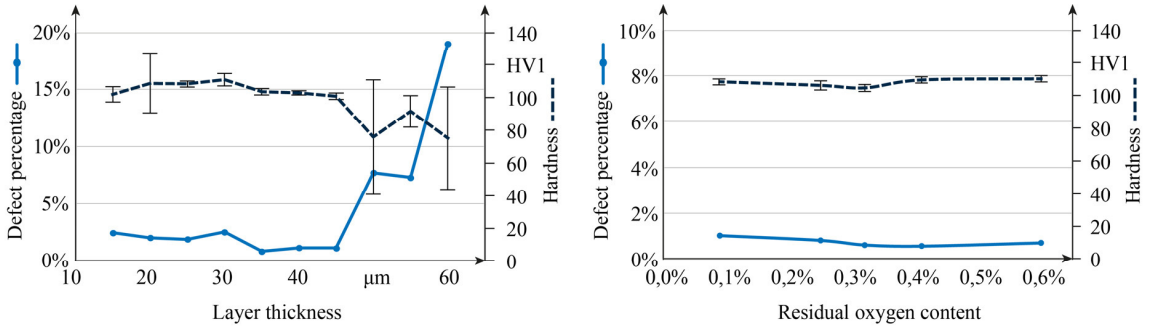

Fig. 10. Defect percentage and hardness values with (a) influence of the layer thickness; (b) influence of the residual oxygen content in process atmosphere.

5. Conclusion

The laser beam melting of AZ magnesium alloys was examined. Single tracks with and without powder were first built to measure process influences with a minimum of disturbance. The influences of the hatch distance on single layers were examined by generating structures with incrementally increasing distance between the laser tracks. The effects of layer height and residual oxygen content were examined, complementing previous studies of process influences on solids. The following conclusions can be drawn:

(1) Keyhole melting occurs when processing magnesium under common LBM parameters.
(2) Sintering is more pronounced for smaller scanning speeds and is probably linked to the evaporations that occur.
(3) Varying energy input by adjusting the layer thickness has a lower effect than varying the hatch distance, scanning speed, or laser power.
(4) No influence on the part-defect percentage or the hardness could be measured when varying the residual oxygen content between 0.1% and 0.6%.
(5) The structure presented by varying the hatch distances can be used to determine influences on surface morphology. A possible direct deviation of process parameters for generating solids seems promising and will be further investigated.

Acknowledgements

The Federal Ministry for Economic Affairs and Energy funded the project based on a decision made by the German Bundestag.

References

Bergström, D., Powell, J., Kaplan, A.F. 2008. The absorption of light by rough metal surfaces-A three-dimensional ray-tracing analysis. Journal of Applied Physics 103 (10). 10.1063/1.2930808.

Boley, C.D., Khairallah, S.A., Rubenchik, A.M. 2015. Calculation of laser absorption by metal powders in additive manufacturing. Applied Optics 54 (9), 2477–2482. 10.1364/AO.54.002477.

Ehrenberger, S. 2013. Life Cycle Assessment of Magnesium Components in Vehicle Construction. German Aerospace Centre e.V. http://www.intlmag.org/newsroom/2013IMA_LCA_Report_Public.pdf.

Gieseke, M., Kiesow, T., Nölke, C., Kaierle, S., Maier, H.J., Haferkamp, H. 2015. Selektives Laserstrahlschmelzen von Magnesium und Magnesiumlegierungen. In: Rapid.Tech - Trade fair and user's conference for Rapid Technology. Tagungsband 2015. DESOTRON, Erfurt.

Gieseke, M., Nölke, C., Kaierle, S., Maier, H.J., Haferkamp, H. 2014. Selective Laser Melting of Magnesium Alloys for Manufacturing Individual Implants. In: Demmer, A. (Ed.), Proceedings / DDMC 2014, Fraunhofer Direct Digital Manufacturing Conference, March 12 - 13, 2014, Berlin. Fraunhofer Verlag, Stuttgart.

Gieseke, M., Nölke, C., Kaierle, S., Wesling, V., Haferkamp, H. 2013. Selective laser melting of magnesium and magnesium alloys. In: Magnesium Technology, pp. 65–68.

Hügel, H., Dausinger, F., Graf, T. 2007. Laser in der Fertigung: Strahlquellen, Systeme, Fertigungsverfahren, 2nd ed. Teubner, Wiesbaden.

King, W.E., Barth, H.D., Castillo, V.M., Gallegos, G.F., Gibbs, J.W., Hahn, D.E., Kamath, C., Rubenchik, A.M. 2014. Observation of keyhole-mode laser melting in laser powder-bed fusion additive manufacturing. Journal of Materials Processing Technology 214 (12), 2915–2925. 10.1016/j.jmatprotec.2014.06.005.

Ng, C.C., Savalani, M.M., Lau, M.L., Man, H.C. 2011. Microstructure and mechanical properties of selective laser melted magnesium. Applied Surface Science 257 (17), 7447–7454. 10.1016/j.apsusc.2011.03.004.

Ng, C.C., Savalani, M.M., Man, H.C., Gibson, I. 2010. Layer manufacturing of magnesium and its alloy structures for future applications. Virtual and Physical Prototyping 5 (1), 13–19. 10.1080/17452751003718629.

Pun, T. 1980. A new method for grey-level picture thresholding using the entropy of the histogram. Signal Processing 2 (3), 223–237. 10.1016/0165-1684(80)90020-1.

Savalani, M.M., Ng, C.C., Man, H.C. 2010. Selective laser melting of magnesium for future applications in the medicine. In: Proceedings - 2010 International Conference on Manufacturing Automation, ICMA 2010, pp. 50–54.

Tandon, R., Madan, D. 2013. Lightweight magnesium parts via laser additive manufacturing. In: Advances in Powder Metallurgy and Particulate Materials - 2013, Proceedings of the 2013 International Conference on Powder Metallurgy and Particulate Materials, PowderMet 2013, pp. 373–379.

Vander Voort, G.F. 2004. ASM Handbook, Volume 09 - Metallography and Microstructures. ASM International, Materials Park.

Wei, K., Gao, M., Wang, Z., Zeng, X. 2014. Effect of energy input on formability, microstructure and mechanical properties of selective laser melted AZ91D magnesium alloy. Materials Science and Engineering: A 611, 212–222. 10.1016/j.msea.2014.05.092.

Witte, F. 2010. The history of biodegradable magnesium implants: a review. Acta biomaterialia 6 (5), 1680–1692. 10.1016/j.actbio.2010.02.028.

Zhang, B., Liao, H., Coddet, C. 2012. Effects of processing parameters on properties of selective laser melting Mg–9%Al powder mixture. Materials & Design 34, 753–758. 10.1016/j.matdes.2011.06.061.